

Pattern fidelity in nanoimprinted films using critical dimension small angle x-ray scattering

Ronald L. Jones
Christopher L. Soles
Eric K. Lin

National Institute of Standards and Technology
Polymers Division
Gaithersburg, Maryland 20899
E-mail: ronald.jones@nist.gov

Walter Hu
Ronald M. Reano*
Stella W. Pang

University of Michigan
Department of Electrical Engineering
and Computer Science
Ann Arbor, Michigan 48109

Steven J. Weigand
Denis T. Keane
John P. Quintana

Argonne National Laboratory
DND-CAT
Advanced Photon Source
Argonne, Illinois 60439

Abstract. The primary measure of process quality in nanoimprint lithography (NIL) is the fidelity of pattern transfer, comparing the dimensions of the imprinted pattern to those of the mold. Routine production of nanoscale patterns will require new metrologies capable of nondestructive dimensional measurements of both the mold and the pattern with subnanometer precision. In this work, a rapid, nondestructive technique termed critical dimension small angle x-ray scattering (CD-SAXS) is used to measure the cross sectional shape of both a pattern master, or mold, and the resulting imprinted films. CD-SAXS data are used to extract periodicity as well as pattern height, width, and sidewall angles. Films of varying materials are molded by thermal embossed NIL at temperatures both near and far from the bulk glass transition (T_G). The polymer systems include a photoresist and two homopolymers. Our results indicate that molding at low temperatures ($T - T_G < 40^\circ\text{C}$) produces small-aspect-ratio patterns that maintain periodicity to within a single nanometer, but feature large sidewall angles. While the observed pattern height does not reach that of the mold until very large imprinting temperatures ($T - T_G \approx 70^\circ\text{C}$), the pattern width of the mold is accurately transferred for $T - T_G > 30^\circ\text{C}$.

© 2006 Society of Photo-Optical Instrumentation Engineers. [DOI: 10.1117/1.2170550]

Subject terms: nanoimprint lithography; critical dimension metrology; x-ray scattering; sub-100-nm lithography.

Paper 05037R received May 2, 2005; revised manuscript received Sep. 26, 2005; accepted for publication Sep. 26, 2005; published online Mar. 28, 2006. This paper is a revision of a paper presented at the SPIE conference on Emerging Lithographic Technologies IX, Mar. 2005, San Jose, California. The paper presented there appears (unrefereed) in SPIE Proceedings Vol. 5751.

1 Introduction

Nanoimprint lithography (NIL) is a low-cost, effective nanofabrication tool for patterning arbitrary structures with critical dimensions (CDs) well below 50 nm. To date, novel patterns with feature sizes smaller than 5 nm have been demonstrated.^{1,2} Representing a potential solution for true nanofabrication, NIL is now listed in the *International Technology Roadmap for Semiconductors* as a potential next-generation lithography for semiconductor fabrication.³ In addition to semiconductors, the potential of NIL to pattern polymers, and perhaps other materials,⁴ of arbitrary chemistry promises to provide a low-cost fabrication alternative to a host of developing technologies, including nanoelectronic machines (NEMS), photonic waveguides, high density storage devices, and microfluidic devices.^{5–8} Fabricating devices with NIL will require precise control over dimensions of the imprinted pattern, even on the level of nanometers. The fidelity of pattern transfer is therefore a critical indication of the suitability of a specific set of NIL parameters, requiring precise dimensional characterization of both the imprinted pattern and the mold. However, cur-

rent metrologies face significant challenges in characterizing pattern fidelity.^{9–11} In particular, the need to examine the original mold in a nondestructive manner restricts the application of traditional imaging techniques such as scanning or transmission electron microscopy. Visible-light-based metrologies also face increasing challenges as feature sizes shrink to an order of magnitude below the probing wavelength.

We have developed a nondestructive metrology capable of subnanometer precision in dimensional measurements. Critical dimension small angle x-ray scattering (CD-SAXS) measures the diffraction from a repeating pattern by transmission x-ray scattering (see Fig. 1). Using x-rays with an appropriate energy (>13 keV), the flux through silicon wafers, glass, and quartz substrates is sufficient to measure most common molds as well as the imprinted patterns. The subangstrom wavelength greatly enhances the ability to extract information on patterned media through diffraction, even in dense patterns of <10 nm in width. This technique has been previously applied to the study of photoresist materials^{12,13}; however, the capability to measure both the mold and the imprinted pattern with identical instrumental parameters makes CD-SAXS an ideal candidate for NIL metrology. Here, we apply CD-SAXS to a critical issue in NIL, namely the fidelity of pattern transfer.

Process parameters that dictate the fidelity of pattern transfer in thermally embossed NIL include imprinting tem-

*Current affiliation: Ohio State Univ., Dept. of Electrical and Computer Engineering, Columbus, OH 43210.

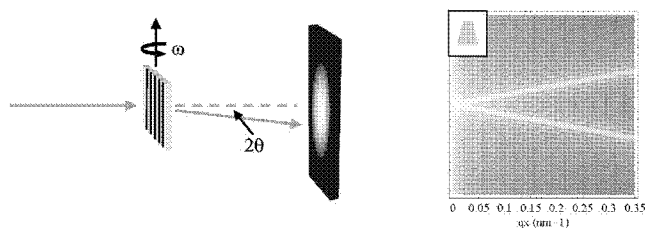


Fig. 1 Schematic of CD-SAXS instrumental geometry (left) showing the x-ray beam (solid thick lines) in transmission through the patterned sample. The intensity I is measured on a 2-D detector as a function of scattering angle 2θ , and converted to $I(q_x)$, where q_x is defined in the text. A series of measurements are performed at varying angles of incidence to the sample, where the sample rotation angle ω is shown. After conversion from the $qx-\omega$ plane, the intensities from a trapezoidal cross section would appear as predicted in the model calculation on the right, plotted as I as a function of the Fourier components, Q_x and Q_z .

perature, pressure, polymer molecular weight, and surface chemistry of the mold.¹⁴⁻¹⁷ A critical issue in NIL is the flow of material into features of dimensions approaching the molecular diameter of the imprinted polymer film. Within these levels of confinement, the rheological properties of high molecular weight polymers are expected to be controlled by the polymer/mold surfaces after flow begins into the mold. The initial stages leading to flow into the mold, where the mold initially deforms the film surface, may be dictated by the surface properties of the unimprinted film. This region may be particularly important when imprinting at small $T-T_G$ and large pressures. Since the resulting patterns in this region are likely to be of small aspect ratio, high precision metrologies of shape and pattern replication are required. As mold filling begins, prior studies using molds with large cavities ($>1 \mu\text{m}$) have shown that the cavity walls fill first, through a capillary wetting mechanism, followed by a filling of the cavity interior.¹⁴ As the cavity size decreases, however, the filling mechanism is completely dictated by the surfaces and becomes similar to “plug flow” found in macroscopic systems. For cavities with widths of $<500 \text{ nm}$, we expect a simple flow that fills the entire width when the polymer readily flows (i.e., $T \gg T_G$). Under these conditions, and relatively vertical sidewalls, the height of the imprinted pattern will depend on the processing variables until complete mold fill is achieved. In contrast, the average values of sidewall angle and line width may be relatively independent of the same variables. Finally, warpage of a pattern, even under optimal conditions, may occur due to residual stresses in the patterns, resulting in restoring forces, and uneven mold removal, resulting in systematic pattern tilt.^{16,18}

Using these observations of the NIL process, it is possible to understand the efficacy of processing parameters simply from a knowledge of the resulting pattern shape. Large-aspect-ratio patterns that mimic the mold dimensions are expected from optimal processing parameters. In this case, the pattern height may be the best indicator of the distance from optimum conditions. Optimal conditions may still result in pattern warpage through restoring forces, while mold removal can serve to cause a systematic tilt across a wide area. In this study, we use CD-SAXS to com-

pare the final shape of a series of polymers imprinted under varying temperatures to the analogous dimensions of a silicon mold.

2 Scattering Model

The diffraction of a collimated x-ray beam passing through a nanoimprinted pattern can be modeled by the relationship $I(\mathbf{Q}) = \Omega F(\mathbf{Q}) F^*(\mathbf{Q})$, where Ω is a \mathbf{Q} independent constant. $F(\mathbf{Q})$ is the Fourier transform of a function describing the relative positions of mass in the pattern, where \mathbf{Q} is the resulting inverse space vector, and $*$ denotes the conjugate value. Approximations used to obtain this form of $I(\mathbf{Q})$ are considered valid in the limits of the CD-SAXS geometry, namely a transmission geometry and a low probability of multiple scattering. A detailed discussion of the CD-SAXS models are provided elsewhere,¹³ and the discussion here is limited to the modeling of pattern fidelity. The loss of phase information in the conjugate product makes an analytical extraction of $F(\mathbf{Q})$ from $I(\mathbf{Q})$ impossible. The primary method of determining dimensions is therefore to build a real space model of the pattern cross section and fit the resulting Fourier transform to the CD-SAXS data.

Using this premise, a real space model cross section of an isolated nanoimprinted line in the real space $x-z$ plane is given in Fig. 1. After Fourier transformation, the predicted scattered intensity is given in the Q_x-Q_z plane. The model line shape used here is a trapezoid characterized by a width W , height H , and two sidewall angles β_1 and β_2 . The width and height are manifested as periodic functions along Q_x and Q_z , respectively, with minima occurring at $W = 2\pi n/Q_x$, where n is an integer, and $H = 2\pi m/Q_z$. The two sidewalls produce characteristic intensity ridges along $Q_z = \beta_1 Q_x$ and $Q_z = -\beta_2 Q_x$. Extending the model of an isolated line to a series of periodically spaced lines results in a series of diffraction peaks at $Q_x = 2\pi/L$, where L is the repeat period of the pattern. While the spacing of the peaks results from the lattice, the relative intensities follow the form of the isolated line predicted in Fig. 1. The model used here is therefore a periodic lattice of trapezoidal lines, with parameters of periodicity, average line width and height, and two sidewall angles. Finally, an excess decay of $I(q_x)$ beyond that predicted by the trapezoidal model is expected from the distribution in periodicity. This distribution can arise from random variations in the average line position, where the line width is constant, or from variations in the line width that also affect the periodicity. In both cases, this factor is indicative of long-range order, and also provides insight into certain types of line edge roughness.¹⁸ Here, this effect is approximated by an effective Debye-Waller factor similar to that derived for fluctuations in crystal lattices. The resulting quantity is the root mean square average of the deviation in periodicity across the beam spot size $\langle \delta L^2 \rangle^{1/2}$, where the brackets indicate an ensemble average. As described here, each of these parameters is independently specified by the form of intensity in the Q_x-Q_z plane.

In this study, a trapezoid model is fit to the experimental data and the parameters of average periodicity, line width, opposing sidewall angles, and pattern height are extracted. In addition, a measure of the deviation in periodicity is also obtained as described before. Here, there is no metric used

Table 1 Results of fitting CD-SAXS data to a trapezoidal cross sectional model. Shown are the samples, their imprinting temperature relative to their bulk glass transition temperature, and the resulting periodicity (L), line width (W), line height (H), sidewall angles (β_1 and β_2), and deviation in periodicity. The values are provided with standard uncertainties. The value of W for the silicon mold represents the width of the space and not the width of the actual line, to provide a clearer comparison with the imprinted patterns.

Sample	$\frac{T_{\text{imprint}}}{T_G}$ (°C)	L (nm)	W (nm)	H (nm)	β_1 (°)	β_2 (°)	$\langle \delta L^2 \rangle^{1/2}$ (nm)
Silicon mold	NA	358.4±0.5	111.5±1.0	167±3	5.6±0.1	5.6±0.1	3.2±0.5
PMMA	≈10	358.4±0.5	105.5±1.0	50±10	10±2	3±2	4.4±1.0
PMMA	≈70	358.4±0.5	111.5±1.0	161±5	2.2±0.5	5.8±0.5	3.0±0.5
PMMA	≈80	358.4±0.5	96.5±1	149±10	-4.0±1	11.1±1	3.5±0.5
PS	≈5	NA	NA	NA	NA	NA	NA
PS	≈45	358.4±0.5	99.5±1.0	151±10	12±1	-6.0±1	3.5±0.5
S1813	≈ (20 to 30)	358.4±0.5	105.5±1	140±1	5.4±0.5	5.6±0.5	3.5±0.5
S1813	≈ (50 to 60)	NA	NA	NA	NA	NA	NA

to determine the validity of this particular model relative to other models. The parameters obtained are therefore considered as resulting from the best-fit trapezoid to the actual structure. Based on the existence of intensity ridges, as described before, resulting from planar faces at specific angles to the vertical plane, and observation of the trapezoidal shape of the line cross sections in scanning electron microscope (SEM) images, we believe this approximation to be valid and the parameters extracted to be quantitative measures of both the mold and the resulting imprints. However, based on the current model, we cannot state that other models, for instance a trapezoid with rounded corners, would not provide a better fit to the data.

Finally, the best fit is based on a minimization of residuals between the experimental data and the model data. To enhance the speed and reliability of the fitting procedure, the step size in parameter estimation was limited to a minimum of 0.1 nm in periodicity, line width, and distribution in periodicity. This limitation is considered valid, given the estimates of error for these quantities, though it is possible that this will affect the fitted values of other parameters. As a result of this minimum step size, the values in Table 1 appear discrete and will not reflect, for instance, differences between a sample with periodicity of 100.08 and 101.04 nm. The errors associated with reported values arise from both instrumental parameters, which do not vary from sample to sample, and estimates of the uncertainty associated with the model fitting, which does vary from sample to sample. Among these, the uncertainty in periodicity and the distribution in periodicity are primarily based on instrumental errors in detector pixel placement and detector distance, and are therefore equivalent for all measurements. Pattern height varies according to, for example, the number and intensity of fringes along the Q_z axis.

3 Experimental Procedure

Polymers used in this study included atactic poly(methyl methacrylate) (PMMA), atactic poly(styrene) (PS), purchased from Microchem Inc. (Newton, MA),¹⁹ and S1813 photoresist from Shipley Company. (Commercial equipment and materials are identified in this work only to adequately specify experimental procedure. In no case does this imply endorsement or recommendation by the National Institute of Standards and Technology.) The PMMA has a number average relative molecular mass ($M_{r,n}$) of 950,000 and polydispersity (PDI) of 2.2, and the PS has $M_{r,n}$ = 50,000 with a PDI=2.1. All films were spun cast from solution on 200-mm-diam silicon wafers and annealed afterward to remove excess solvent. The resulting film thicknesses were measured by profilometry and found to be ≈310 nm for both the PMMA and PS, and ≈260 nm for the S1813. The nanoimprint mold consists of a set of parallel lines and spacings with a line to space ratio of approximately 3:1. The line-space pattern covers a square with sides of 5 mm. CD-SAXS measurements were performed near the center of the imprinted area. The mold was fabricated in silicon oxide via 193-nm photolithography using a JSR 1237R resist on a 200-mm SEMI-standard Si wafer. Nanoimprint lithography was performed on an Obducat NIL 4 (Series 1) machine. Imprinting was conducted in the thermal embossing mode for 10 min at a pressure of 6 MPa. Subsequently, the mold was cooled to below T_G before the sample was removed from the mold. For each sample, SEM images were taken of identically prepared samples after cleaving to provide cross sectional views of the patterns. The SEM images reveal a residual, unpatterned layer that is >100 nm thick in all samples.

CD-SAXS experiments were performed at the 5-ID-D beamline of the DND-CAT at the Advanced Photon Source,

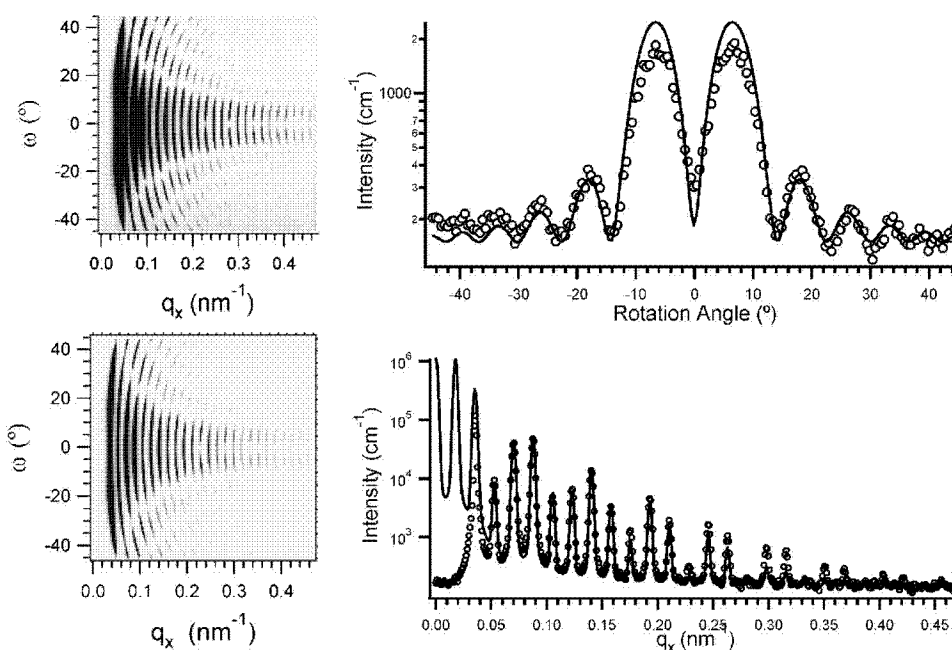


Fig. 2 CD-SAXS data from a silicon master (top left) shown as a function of ω and q_x is compared to analogous data from a 2-D model of a trapezoidal cross section (bottom left). Also shown is a comparison of intensity contours from experiment (open circles) and the model (solid line) at constant $q_x=0.225 \text{ nm}^{-1}$ (top right) and constant $\omega=-0.4^\circ$ (bottom right).

part of Argonne National Laboratory (Argonne, Illinois). An x-ray energy of $E=17 \text{ keV}$ was selected using a double monochromator, corresponding to a wavelength of $\lambda=(0.0729\pm 0.0001) \text{ nm}$. At this wavelength, silicon wafers used in microelectronic fabrication, with total thickness $\approx 0.5 \text{ mm}$, have a transmission of ≈ 0.45 . The sample is oriented with the pattern on the detector side to reduce the possibility of beam damage. While we have not systematically studied the effects of the beam on the polymers used here, we note that we have not observed changes in pattern shape for other polymer-based samples after exposures of more than 4 h. Diffraction of the pattern is recorded on a 2-D charge-coupled device (CCD) detector with 2048×2048 pixels. The detector was set at a distance of $(700\pm 1) \text{ cm}$ from the sample. Intensities were recorded as a function of the scattering vector \mathbf{q} [$=4\pi/\lambda \sin(\theta)$, where 2θ is the angle of diffraction as depicted in Fig. 1]. The values of \mathbf{q} measured were calibrated using the diffraction of a grating of period of 400 nm , previously calibrated by comparison with the diffraction from the 100 plane of silver behenate. The capability to calibrate SAXS to a traceable standard is an inherent advantage of scattering-based techniques over imaging-based platforms. Mapping of the Q_x - Q_z plane described before requires a series of measurements at varying angles of sample rotation ω . The relationship $\mathbf{I}(Q_x, Q_z)=\mathbf{I}(q, \omega) \mathbf{R}(\omega)$, where \mathbf{R} is a rotation matrix projecting the vector \mathbf{q} into the Q_x - Q_z plane, is then used to transform the data into the sample coordinate system.

The x-ray beam was characterized by scanning a photo-sensitive diode across the beam path along the sample plane. The beam was found to be approximately Gaussian with a width at half the maximum intensity of $\approx 100 \mu\text{m}$ in both horizontal and vertical directions. Based on the square slits used, the beam is expected to be approximately square

rather than pinhole in shape. Locating the beam on the sample was performed using a video microscope focused on the pattern surface. Beam position was nominally placed at the center of the 5×5 -mm patterned area for each sample. A series of measurements of the mold at varying positions near the center of the patterned area did not find differences in scattered intensity outside of the error bars; however, scans were not performed over larger areas or near the edges of the patterned area. A similar scan of the imprinted structures, providing an estimate of the variation in imprint fidelity within the patterned area, has not been performed here.

4 Results and Discussion

CD-SAXS measurements from a silicon oxide master are shown in Fig. 2. The cross section of the pattern is obtained by fitting the diffracted intensity of the pattern to the form of a model cross section over a wide range (-45 to $+45^\circ$) of incident angles. Both experimental and resulting model data are plotted as a contour map of intensity in the ω - q_x plane. Prominent in this form of the data are the Bragg diffraction peaks along the q_x axis. As the sample is rotated, the Bragg peak positions smoothly vary with the projected repeat distance. The maximum period defines the condition of a beam at normal incidence to the plane of the pattern. The intensity ridges created by the sidewalls can be observed at $\omega=\beta_1$ and $\omega=\beta_2$, providing a direct measure of the sidewall angles. Visual examination of the data in Fig. 2 therefore supports the validity of the trapezoidal cross section as a model of the mold. The fitted dimensions of the mold, and subsequent imprints, are given in Table 1. We note that the conservation of length scales between periodicity, line width, and space width results in two identical solutions, representing values for W and $L-W$. Distinguish-

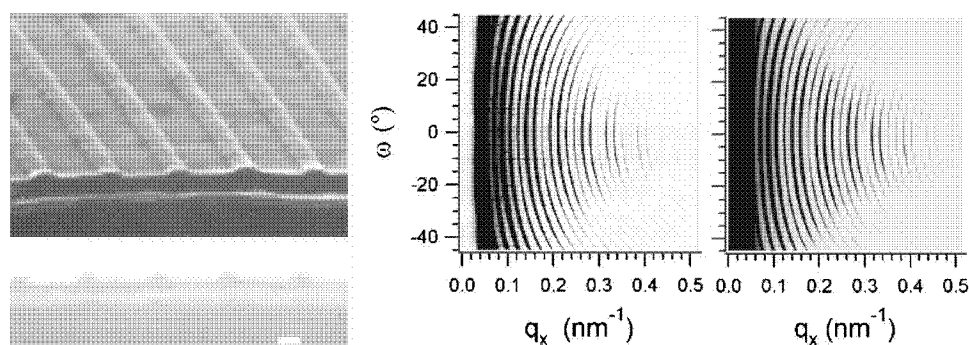


Fig. 3 Cross section SEM images of a line-space pattern imprinted into a PMMA film (left). The white bar represents a scale of 100 nm. In addition, CD-SAXS data from an identically prepared sample is shown as a function of rotation angle ω and q_x (middle), and compared to the resulting model prediction using the trapezoidal cross section (right).

ing between the two solutions using CD-SAXS alone requires additional analysis described elsewhere.¹⁰ Here, the mold is known to have a 3:1 ratio of line and space width, and the line width is assigned the larger value. A similar redundancy exists in the vertical orientation of the trapezoid; however, the nature of the NIL process usually limits molds to structures with positive sidewall angles. Finally, while CD-SAXS provides a value of average periodicity with subnanometer precision, we note that the distribution of periodicity is measured to be $\langle \delta L^2 \rangle^{1/2} = 3$ nm. It is important to realize that this distribution must be included in any direct comparison between average techniques, such as CD-SAXS, and microscopies that examine individual or small numbers of features. In addition to variations in line position, where the lines are otherwise perfect, the Debye-Waller factor will reflect the presence of defects. However, a quantitative connection between types of defects and this factor will require further investigation. Regardless, the Debye-Waller factor is an indication of the density of defects in long-range periodicity and provides a basis for comparison in subsequent imprints.

In Fig. 3, SEM images of a pattern imprinted into PMMA are shown in both “top down” and cross sectional views. Here, the patterns have been imprinted at a small $T-T_G$ ($=10^\circ\text{C}$). Given the high molecular weight of the polymer, it is not surprising that the mold does not fill completely and patterns with a small aspect ratio result. Prior studies of thermally embossed NIL have typically used values of $T-T_G \approx 100^\circ\text{C}$ as a result, even for polymers of lower molecular weight.¹⁷ Nevertheless, the diffraction peaks from an identically prepared sample show that the long-range order of the mold has been successfully transferred, maintaining the same periodicity to within a single nanometer with only a small increase in the Debye-Waller factor (≈ 1 nm). The lack of visually sharp ridges in the 2-D map results from a combination of a low pattern height, broadening the intensity ridges from the sidewalls, and possibly a large distribution in sidewall angle among the lines (see Fig. 3). As may be expected, the trend toward low-aspect-ratio patterns continues with the imprinting of a PS sample at $T-T_G \approx 5^\circ\text{C}$. While SEM images indicate a pattern exists on the PS sample, with a height on the order of 10 nm, CD-SAXS did not detect any diffraction peaks. The lack of diffraction may be due in part to a vanishingly

small pattern size, but may also reflect a high density of defects in the patterns. From this data, we suggest that a minimum positive value of $T-T_G$ on the order of 10°C may be required to create a pattern with long-range order. However, even largely nonoptimal conditions of imprinting serve to reproduce the basic dimensions laterally, resulting in only a 6-nm decrease in average line width for the PMMA sample. A capability to produce patterns with varying aspect ratio, simply by changing temperature, may be useful to produce, for instance, surfaces with controlled morphology. Surface morphology control could play a role in applications such as in nanostructured surfaces for lubrication, bottom-up assembly, and morphologically induced mixing in microfluidic channels. The strong diffraction from the PMMA sample suggests that small-aspect-ratio patterns can be characterized sufficiently with CD-SAXS, provided that a sufficient degree of long-range order exists.

The disparity in dimensions between the mold and the low-temperature PMMA and PS samples is likely due to difficulties in flowing a polymer at temperatures approaching the T_G . To achieve highly conformal imprints, large values of $T-T_G$ ($\approx 40^\circ\text{C}$ or larger) are suggested for many commercial NIL imprinters. In Fig. 4, data from both PS and PMMA films imprinted at higher temperature demonstrate significant increases in pattern height and follow the dimensions of the mold very closely. The heights of the patterns are all within 20 nm of the original mold, but the high aspect ratio also makes the patterns subject to systematic leaning. For the case of a PMMA pattern imprinted at $T-T_G=70^\circ\text{C}$, the pattern remains relatively vertical with two positive sidewall angles, and replicates the mold’s dimensions to within 1 and 6 nm in width and height, respectively. These results suggest that the temperature, time, and pressure are nearly optimal for this polymer. For the PS and a subsequent PMMA imprint, the dimensions also approximate those of the mold; however, tilting of the lines is significant enough to make one of the sidewall angles negative. Since the CD-SAXS data represent an average over hundreds of lines, this tilting occurs systematically over a large ($100 \times 100\text{-}\mu\text{m}$) area and is therefore likely to be caused during mold removal.

The generality of NIL as a nanofabrication tool is further illustrated in Fig. 5, where a photoresist (Shipley S1813) film is imprinted at $T=130^\circ\text{C}$. While the photosensitive

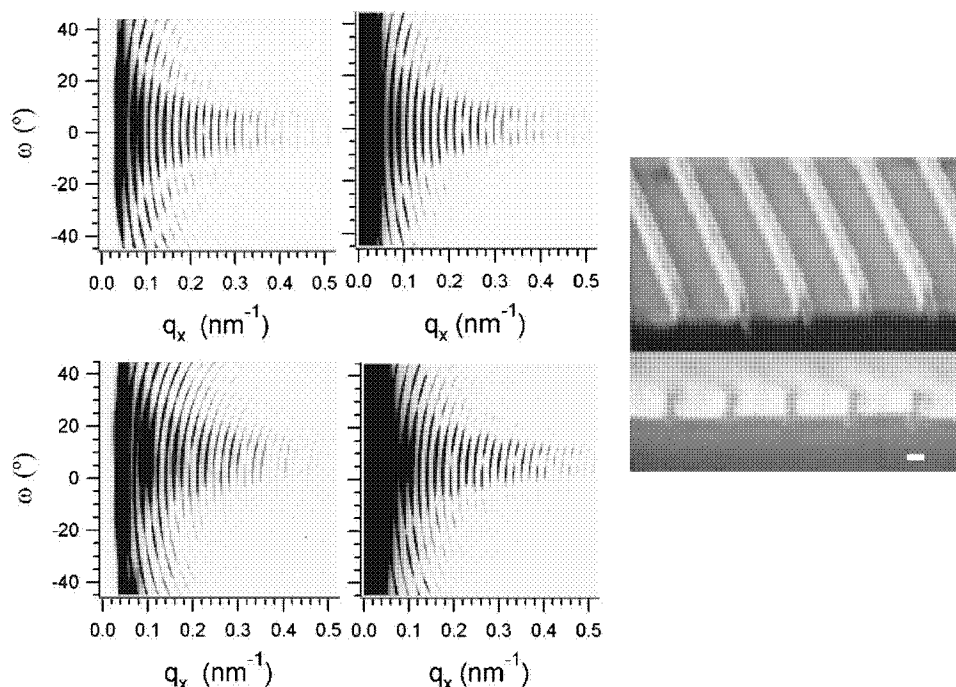


Fig. 4 CD-SAXS data from nanoimprinted PMMA films shown as a function ω and q_x . Shown are data from a film imprinted at $T-T_G=70^\circ\text{C}$ (top left) and $T-T_G=80^\circ\text{C}$ (bottom left). Data are compared to results of fitting to a trapezoidal model for each film (middle) and cross sectional SEM of a sample prepared under nominally identical conditions (right). The white bar represents a length scale of 100 nm in the SEM images.

nature of a photoresist is not required for thermally embossed NIL, the chemical compositions of photoresists are naturally tuned to possess high etch resistance. NIL of photoresists could therefore provide the dimensions required of next-generation lithography while maintaining the established etch properties of photoresists. As with the simpler homopolymers, the resist system shows conformality at $T-T_G > 20^\circ\text{C}$, maintaining periodicity and line width. In addition, this particular sample shows conformality in sidewall angle. The SEM images of Fig. 5 further demonstrate a capability to control pattern aspect ratio simply through temperature.

The limitations of CD-SAXS are general to techniques that provide average measures, namely an inability to see small concentrations of defects, especially when the defects are not spatially correlated. Further development of the technique will attempt to provide quantitative measures of the distributions in each of these parameters, in a manner

similar to the Debye-Waller factor in the periodicity, as well as addressing more complex cross sectional shapes. Given the transmission geometry of the technique, and its capability to do measurements on the time scale of seconds,¹⁸ it is also conceivable that *in-situ* measurements are possible, directly following the flow of material into the mold, provided that a nanoimprinter can be placed or manufactured around a suitable source.

5 Conclusions

A technique based on transmission x-ray scattering, termed critical dimension small angle x-ray scattering (CD-SAXS) is used to characterize the fidelity of pattern transfer in thermally embossed NIL patterns. Line/space patterns with 1:3 spacing are imprinted in films of PMMA, PS, and S1813 photoresist, and their cross section characterized nondestructively. Dimensions are compared to analogous

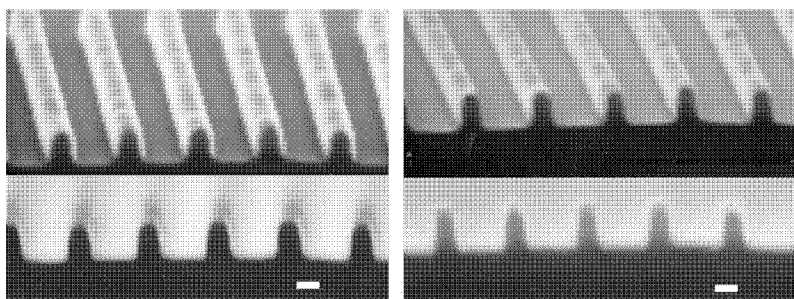


Fig. 5 Cross section SEM images of two S1813 films imprinted at $T-T_G= (20 \text{ to } 30)^\circ\text{C}$ and $T-T_G= (60 \text{ to } 70)^\circ\text{C}$. Images show a small increase in pattern height with increasing temperature. The white bar represents 100 nm in the SEM images.

measurements of the silicon oxide master and cross sectional SEM of nominally identically prepared imprints. Patterns are modeled with a trapezoidal cross section, providing subnanometer precision in periodicity, nanometer level precision in pattern width and height, and subdegree precision in sidewall angle. Incomplete fill of the mold was observed in PMMA and PS imprinted at $T-T_G < 15^\circ\text{C}$, suggesting a potential route toward control over pattern height with a single mold. Patterns imprinted at $T-T_G > 40^\circ\text{C}$ filled the mold to within 20 nm of the height of the mold patterns. The technique also reveals slight tilts in the resulting structures, likely due to deformation during mold release, as well as sensitivity to more complex cross sections. Finally, the transmission geometry of CD-SAXS suggests the possibility of nondestructive, *in situ* metrology of the molding process.

Acknowledgments

Funding for this research was provided by the National Institute of Standards and Technology (NIST) Office of Microelectronic Programs. This work was funded in part by the NIST Office of Microelectronic Programs and the National Institute of Health. The Advanced Photon Source is supported by the U.S. Department of Energy under contract number W-31-109-Eng-38. The mold was provided by A. Mahorowala of the IBM T. J. Watson Research Center, Yorktown Heights, New York.

References

1. M. D. Austin, H. Ge, W. Wu, M. Li, Z. Yu, D. Wasserman, S. A. Lyon, and S. Y. Chou, "Fabrication of 5 nm linewidth and 14 nm pitch features by nanoimprint lithography," *Appl. Phys. Lett.* **84**(26), 5299–5301 (2004).
2. F. Hua, Y. Sun, A. Gaur, M. A. Meitl, L. Bilhaut, L. Rotkina, J. Wang, P. Geil, M. Shim, and J. A. Rogers, "Polymer imprint lithography with molecular-scale resolution," *Nano Lett.* **4**(12), 2467–2471 (2004).
3. 2004 International Technology Roadmap for Semiconductors, see <http://www.public.net/itrs>.
4. C. D. Schaper, "Patterned transfer of metallic thin film nanostructures by water-soluble polymer templates," *Nano Lett.* **3**(9), 1305–1309 (2003).
5. H. Kostal, "Nanostructures benefit telecom," *OE Mag.* **2**(8), 18 (2002).
6. K. Watanabe, T. Morita, R. Kometani, T. Hoshino, K. Kondo, K. Kanda, Y. Haruyama, T. Kaito, J. Fujita, M. Ishida, Y. Ochiai, T. Tajima, and S. Matsui, "Nanoimprint using three-dimensional micro-lens mold made by focused-ion-beam chemical vapor deposition," *J. Vac. Sci. Technol. B* **22**(1), 22–26 (2004).
7. H. Cao, Z. Yu, J. Wang, J. O. Tegenfeldt, R. H. Austin, E. Chen, W. Wu, and S. Y. Chou, "Fabrication of 10 nm enclosed nanofluidic channels," *Appl. Phys. Lett.* **81**(1), 174–176 (2002).
8. L. J. Guo, X. Cheng, and C. F. Chou, "Fabrication of size-controllable nanofluidic channels by nanoimprinting and its application for DNA stretching," *Nano Lett.* **4**(1), 69–73 (2004).
9. D. C. Joy and G. F. Lorusso, "Experimental resolution measurement in critical dimension scanning electron microscope metrology," *Scanning* **25**(4), 175–180 (2003).
10. W. D. Yang, J. T. Hu, R. Lowe-Webb, R. Korlahalli, D. Shivaprasad, H. Sasano, W. Liu, and D. S. L. Mui, "Line-profile and critical dimension monitoring using a normal incidence optical CD metrology," *IEEE Trans. Semicond. Manuf.* **17**(4), 564–572 (2004).
11. T. H. Huang and F. L. Terry, "Spectroscopic ellipsometry and reflectometry from gratings (Scatterometry) for critical dimension measurement and in situ real-time process monitoring," *Thin Solid Films* **455–456**(1), 828–836 (2004).
12. R. L. Jones, T. Hu, E. K. Lin, W. L. Wu, R. Kolb, D. M. Casa, P. J. Bolton, and G. G. Barclay, "Small angle x-ray scattering for sub-100 nm pattern characterization," *Appl. Phys. Lett.* **83**(19), 4059–4061 (2003).
13. T. Hu, R. L. Jones, W. L. Wu, E. K. Lin, Q. Lin, D. Keane, S. Weigand, and J. P. Quintana, "Small angle x-ray scattering metrology for sidewall angle and cross section of nanometer scale line gratings," *J. Appl. Phys.* **96**(4), 1983–1987 (2004).
14. L. J. Heyderman, H. Schiff, C. David, J. Gobrecht, and T. Schweizer, "Flow behavior of thin polymer films used for hot embossing lithography," *Microelectron. Eng.* **54**(3–4), 229–245 (2000).
15. H. D. Rowland and W. P. King, "Polymer deformation and filling modes during microembossing," *J. Micromech. Microeng.* **14**(12), 1625–1631 (2004).
16. S. Zankovych, T. Hoffmann, J. Seekamp, J. U. Bruch, and C. M. Sotomayor Torres, "Nanoimprint lithography: challenges and prospects," *Nanotechnology* **12**(2), 91–95 (2001).
17. H. C. Scheer and H. Schulz, "A contribution to the flow behaviour of thin polymer films during hot embossing lithography," *Microelectron. Eng.* **56**(3–4), 311–332 (2001).
18. R. L. Jones, C. L. Soles, T. Hu, E. K. Lin, W. Hu, R. M. Reano, S. W. Pang, and D. M. Casa, *Nano Lett.* (in press).
19. Commercial equipment and materials are identified in this paper only to adequately specify experimental procedure. In no case does this imply endorsement or recommendation by the National Institute of Standards and Technology.

Biographies and photographs of the authors not available.